Available online at www.sciencedirect.com
ScienceDirect
International Journal of Heat and Mass Transfer 50 (2007) 3100–3114
International Journal of HEAT and MASS TRANSFER
www.elsevier.com/locate/ijhmt

Effect of developing flow and thermal regime on momentum and heat transfer in micro-scale heat sink

Y. Mishan, A. Mosyak, E. Pogrebnyak, G. Hetsroni *

Department of Mechanical Engineering, Technion-Israel Institute of Technology, Haifa 32000, Israel

Received 28 August 2006
Available online 27 February 2007

Abstract

A developing micro-channel heat transfer and fluid flow has been investigated experimentally in rectangular micro-channels of $D_h = 440$ μm, having water as a working fluid. Infrared technique was used to design and built a micro-channel test section that incorporate internal fluid temperature measurements. The new method that provides information about the fluid temperature distribution inside the channel and provides validation for the methods used to determine the local and average Nusselt numbers. The experimental results have been compared with theoretical predictions from the literature and results obtained by numerical modeling of the present experiment. The experimental results of pressure drop and heat transfer confirm that including the entrance effects, the conventional theory is applicable for water flow through micro-channels.

These results differ from the conclusions of several researches. It was shown that data presented by some researches can be due to entrance effects. The present results highlight the importance of accounting for common phenomena that are often negligible for standard flows such as accounting for profile of inlet velocity, axial heat conduction, effect of the design inlet and outlet manifolds.

This paper, to the best of knowledge, is the first presentation on the method of the bulk fluid temperature measurements along micro-channel using IR technique, and calculation of the local heat transfer coefficient based on the local heat flux and the local temperature difference between the heated wall and the bulk fluid temperature.

Keywords: Micro-channels; Laminar flow; Entrance effect; Axial conduction; Infrared technique; Pressure drop; Heat transfer

1. Introduction

One potential solution to thermal management of a chip is to attach a micro-channel heat sink to inactive (back) side of the chip. Usually in a close-loop arrangement, coolant such as water is pumped trough the micro-channels to remove the heat generated. Due to the small size of the micro-channels, the heat transfer coefficient is very high. In an early work by Tuckerman and Pease [1], a micro-channel heat sink consisting of parallel micro-flow passages, was demonstrated to have very small thermal resistance. Since that time, this technology has been used in micro-electronics and other major application areas, such as fuel cell systems and advanced heat sink designs. These practical advantages of micro-channel heat sinks have stimulated researches in experimental, theoretical and also numerical field. Comprehensive surveys may be found in [2–5]. Experimental studies on micro-channel heat transfer and pressure measurements reported in the literature present strong dispersion of the results and sometimes disagree with the conventional theories of transport phenomena which are well verified in macro-scale flows.

Effect of entrance length on the pressure drop and the heat transfer for conventional channels was presented by Shah and London [6]. Kim and Kim [7] investigated numerically the influence of velocity and temperature distributions on the heat transfer and friction factor at both high-aspect-ratio and low-aspect-ratio micro-channels heat

* Corresponding author. Tel.: +972 48 292058; fax: +972 48 238101.
E-mail address: hetsroni@techunix.technion.ac.il (G. Hetsroni).

0017-9310/$ - see front matter © 2007 Elsevier Ltd. All rights reserved.
doi:10.1016/j.ijheatmasstransfer.2006.12.003

Nomenclature

A	cross-section area
C_p	specific heat
C^*	Po_{exp}/Po_{th}
D	diameter
f	friction factor
F	heated surface
h	heat transfer coefficient
H	micro-channel height
k_f	thermal conductivity of the fluid
k_s	roughness
K_∞	developing flow loss coefficient
L	length
$\dot{m}$	mass flux
N	power
Nu	Nusselt number
P	pressure
Pe	Peclet number
Po	Poiseuille number
Pr	Prandtl number
q	heat flux
Re	Reynolds number
r_0	micro-channel hydraulic radius
T	temperature
u	velocity
u^*	friction velocity
W	micro-channel width
x, y, z	Cartesian coordinates
X^+	dimensionless hydraulic entrance length
X^*	dimensionless thermal entrance length

Greek symbols

α	aspect ratio
ε	uncertainty
η	dimensionless radius
μ	dynamic viscosity
ν	kinematic viscosity
ρ	density
τ	shear stress

Subscripts

av	average
exp	experimental
f	fluid
h	hydraulic
in	inner
T	thermal
th	theoretical
w	wall

sinks. Petukhov [8] investigated heat transfer characteristics and drag of laminar flow of liquid in pipes.

Peng and Peterson [9] and later, Peng and Wang [10] investigated the convective heat transfer and flow friction for water flow in micro-channel structures. The experimental results indicated that the geometric configuration had a significant effect on the single-phase convective heat transfer and flow characteristics. Empirical correlations were suggested for calculating both the heat transfer and pressure drop.

Qu et al. [11] performed an experimental study of the pressure drop in trapezoidal silicon micro-channels with a hydraulic diameter ranging between 51 μm and 169 μm. A high ratio of channel length to diameter $180 < (L/D_h) < 600$ determined fully developed laminar flow regime in which, the calculated friction factors found to be higher, by 8–38% than the expected values obtained by using the conventional theory. The authors justify the deviation in the results due to high relative roughness (3.5–5.7%) in the channel surface and proposed the numerical roughness–viscosity model to explain the experimental data.

Pfund et al. [12] measured the pressure drop, friction factor and Poiseuille number of water flowing along $(D_h) = 128$–1050 μm rectangular micro-channels, at $Re = 60$–3450. In the laminar regime ($Re < 2000$) their data show good agreement with the conventional theory with regard to the non-dependence of Poiseuille number on Reynolds number but the measured values were higher than these corresponding to theoretical prediction.

Jiang et al. [13] investigated frictional losses in rectangular micro-channels of $D_h = 300$ μm. The average value of the non-uniform relative roughness was measured by electron microscope and was found to be as high as 12%. The measured friction factors were larger than the values predicted by the conventional theory. This result was attributed to channel walls roughness and short length of the micro-channels, which did not allow one to neglect the effects of the hydrodynamic entrance region.

Mala and Li [14] investigated experimentally the pressure losses in micro-channels with diameters ranging from 50 μm to 254 μm. The relative roughness changed from 1.36% to 7.0%. The measurements indicated the existence of significant divergence between experimental values of pressure gradient and values predicted by conventional theory.

The effect of roughness on pressure drop in micro-tubes with diameter 620 μm and 1067 μm and relative roughness 0.71%, 058% and 0.321% was investigated by Kandlikar et al. [15]. For 1067 μm diameter tube, the effect of roughness was insignificant. For the 620 μm tube the pressure drop results showed dependence on the surface roughness.

Xu et al. [16] investigated deionized water flow in micro-channels with hydraulic diameter from 30 μm to 344 μm at $Re = 20$–4000. Two different experimental test modules

were used. The first was made of rectangular, aluminum-based channels with a plastic cover attached to the channels top surface by glue. The second one consisted of silicon channels covered by Pyrex glass using anodic bonding. Results obtained showed that deviation from classical correlations reported in earlier studies may have resulted from errors in the measurements of micro-channel dimension, rather than any micro-scale effects.

Sharp and Adrian [17] investigated the transition from laminar to turbulent flow in liquid filled glass microtubes having diameters between 50 μm and 247 μm. The results of more than 1500 measurements of pressure drop vs. flow rate confirm the macroscopic Poiseuille flow result for laminar flow at Reynolds numbers less than 1800.

Guo and Li [18] studied the size effect on micro-scale single-phase flow and heat transfer. Because the micro-devices have a large surface to volume ratio, factors related to surface effects have more impact on the flow at small scales. Among these are surface roughness channel surface geometry and measurement errors. Discrepancies between experimental results for the friction factor and the Nusselt number and their standard values due to the measurement errors might be misunderstood as being caused by novel phenomena at micro-scales.

New method for pressure measurements was reported recently by Kohl et al. [19]. The main objective of this study was to investigate the discrepancies in previously published data, by using straight channel test section with integrated miniature pressure sensors along the flow direction. The channel hydraulic diameter was $D_h = 25$–100 μm under incompressible flow conditions and $Re = 4.9$–2068. This unique technique allows one to consider entrance effects and hydrodynamic developing flow for pressure drop calculations. The results suggested that friction factors for micro-channels can be accurately determined from data for standard large channels. The authors explain the large inconsistencies in previous researches, probably, due to instrumentation errors and/or improper accounting for compressibility effects. In addition, the pressure drop inside the channel associated with the developing flow was found to be as large as 17% of the pressure drop inside the channel, therefore, it is important to include this effect, especially for the channels with $L/D_h < 300$.

Klein et al. [20] and Zhang and Li [21] demonstrated the importance of the micro-channel manifolds design and the influence on the velocity and temperature fields, both, in the flowing cooling liquid and on the heated wall.

Hetsroni et al. [22] measured the surface temperature of a heated capillary tube by means of an infrared technique in order to determined the average and local heat transfer coefficient in laminar flow.

Rahman [23] tested the forced convection of water in etched silicon micro-channels with $D_h = 300$–490 and $90 < L/D_h < 150$. The main results of this study showed that the measured values of the average Nusselt number are usually larger than those predicted by correlations for large size channels. The author explained this finding as being caused by the breakage of the velocity boundary layer by surface roughness associated with the channel structure.

Tiselj et al. [24] investigated the effect of axial conduction on the heat transfer in micro-channels. Experimental and numerical analysis were performed to evaluate heat transfer characteristics of water flowing through triangular silicon micro-channels. It was shown that as the bulk water temperature, as well as the temperature of the heated wall, do not change linearly along the channel.

Simultaneously developing three-dimensional laminar flow and heat transfer in the entrance region of trapezoidal channels have been investigated by Renksizbulut and Niazmand [25] using numerical methods in the Reynolds number range from 10 to 1000. The results for the fully developed flow region of the channels compare well with the available literature. It was shown that Reynolds-number-independent Poiseuille number can be used for Reynolds numbers over 50 and after a few hydraulic diameters from the channel inlet. It was also shown that hydrodynamic entrance lengths calculated with methods based on fully developed flow data are grossly in error.

Qu and Mudawar [26] studied both experimentally and numerically heat transfer characteristics of a single-phase micro-channel heat sink. The heat sink consisted of an array of rectangular, oxygen-free copper, channels, 231 μm wide and 713 μm deep. The Reynolds number ranged from 139 to 1672. The experimental results were compared with the numerical predictions by considering the conjugated heat transfer between the solid and the fluid region. The measured temperature distributions showed good agreement with the corresponding numerical predictions.

Lelea et al. [27] experimentally researched the heat transfer and fluid flow in microtubes having diameters of 0.1, 0.3 and 0.5 mm. The cooling liquid in use was distilled water in the laminar flow regime. Special care has been taken for reducing the heat loss in order to keep experimental uncertainty within an allowable level for the thermal results.

Warrier et al. [28] conducted experiments of forced convection in small rectangular channels using FC-84 as test fluid. The test section consisted of five parallel aluminum-based channels, with hydraulic diameter of $D_h = 0.75$ mm and length to diameter ratio of $L/D_h = 433.5$. Experimental results of the variation of local Nu as a function of the axial distance were compared to numerical data presented by Kays and Crawford [29] and agree quite well, especially near the fully developed region. In addition, the authors measured the experimentally Fanning friction factors and found them about 8–14% higher than the analytically predicted values.

The influence of size effects and scaling on hydrodynamic flow and heat transfer in 2-D micro-channels was investigated by Gao et al. [30]. The test section consisted of a single bronze micro-channel with hydraulic diameter ranging from 200 μm to 2 mm, the ratio of the length to hydraulic diameter was $40 < L/D_h < 400$, and the aspect ratio (depth to width ratio) was $0.004 < H/W < 0.04$. The local Poiseuille number expressed as a function of

$L^* = L/(D_h \cdot Re)$ was compared with the theoretical solution for laminar flow regime and the results demonstrate good agreement. However, for the lowest aspect ratio ($H/W = 0.004$) the plot Nu_x shows departure from the theoretical heat transfer trend and found to be smaller (reduction of 60%) than the conventional value for large scale channels reported by Shah and London [6]. The researchers rejected roughness and electro kinetics effects in attempt to find an explanation for these findings.

In a continuance study, Gamrat et al. [31] based their numerical investigation on the same experimental facility used by Gao et al. [30] and built a 3-D model for solving simultaneously the fluid flow and energy equations. They considered thermal entrance effects and coupling conduction–convection condition in order to accurately compare between the measured and computed heat flux and temperature fields. Contrary to the experimental work, the numerical analysis did not reveal any significant size effect on heat transfer down to the smallest hydraulic diameter which was tested.

Xu et al. [32] experimentally investigated a new model, composing of parallel longitudinal and several transverse micro-channels which separate the whole flow length into several independent zones, in which the thermal boundary layer is in developing regime. The redeveloping flow repeated for each region separately, thus the overall heat transfer is greatly increased and the pressure drops are decreased compared with the conventional micro-channel heat sink. Resulted from the shortened "effective flow length", the new structure achieved a significant reduction in pressure drops while enhancing heat transfer. The study discussed the influence of the thermal conduction of the solid silicon on the heating area temperature distribution and on the local Nusselt number.

In order to explore the validity of classical correlations based on large size channels for predicting the thermal behavior in single-phase flow, Lee et al. [33] studied deionized water flow through parallel array of copper micro-channels. The channel width ranged from 194 μm to 534 μm with channel depth being nominally five times the width in each case and Reynolds number range of 300–3500. Numerical predictions obtained based on a classical, continuum approach were found to be in good agreement with the experimental data. The authors noted that the entrance and boundary conditions imposed in the experiment need to be carefully matched in the predictive approaches. It is noteworthy that several studies exhibit contradictory results for both the mechanical and thermal characteristics of the flow. This is generally due to differences in the many parameters that characterize these studies such as the geometry, the shape and surface roughness of the channels, the fluid nature, the boundary conditions and the measuring methodology itself. The micro-channels utilized in engineering are frequently connected with inlet and outlet manifolds and should be considered as micro-scale heat exchangers. In this case the thermal boundary condition at the inlet and the outlet of the channels is not adiabatic. The effects of simultaneously developing flow and thermal regime or hydrodynamically developed but thermally developing regime play an important role. Moreover, uneven flow distribution among parallel micro-channels should be taken into account. It should be stressed that in all experimental investigations in micro-channels the temperature distribution of the working fluid along the heated surface was not measured. In many cases the use of heat transfer model based on the assumption of constant heat flux, and linear variation of the bulk temperature of the fluid at low Reynolds number, yield an apparent growth of the Nusselt number with increase in Reynolds number. For a fundamental insight on the entrance effects on flow and heat transfer into micro-scale cooling devices it is useful to reduce as much as possible the number of parameters.

In the present study we chose geometry of the inlet and outlet manifolds that made it possible for uniform flow distribution among parallel micro-channels, we kept the same surface roughness and measured the fluid bulk temperature along the heated surface. The objective of the present investigation is to study the effect of developing flow and thermal regime on momentum and heat transfer in micro-scale heat sink.

2. Experimental set-up and procedure

A scheme of the experimental apparatus is shown in Fig. 1. Filtered water at room temperature was used as the working fluid. The water was pumped from the entrance tank by a miniature gear pump through the inlet calm chamber, inlet manifold to the micro-channels in the test module, and from the micro-channels through the outlet manifold, outlet calm chamber to the exit tank. The test section is shown in Fig. 2. The mass flow rate of the water was measured by a precision flow meter which was calibrated by a standard weighting method.

2.1. Test module

The test module was fabricated of 14 mm × 20 mm and 1.25 mm thick aluminum plate. The cross-section of the

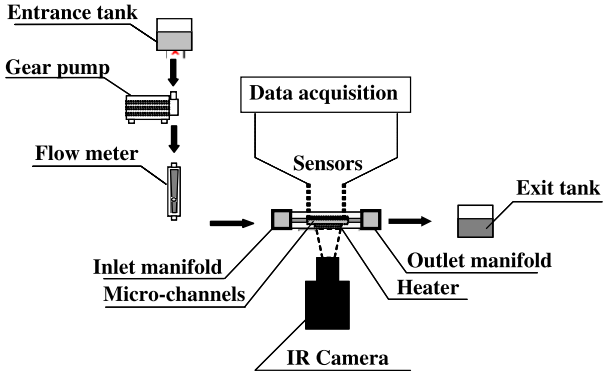

Fig. 1. Experimental set-up and apparatus.

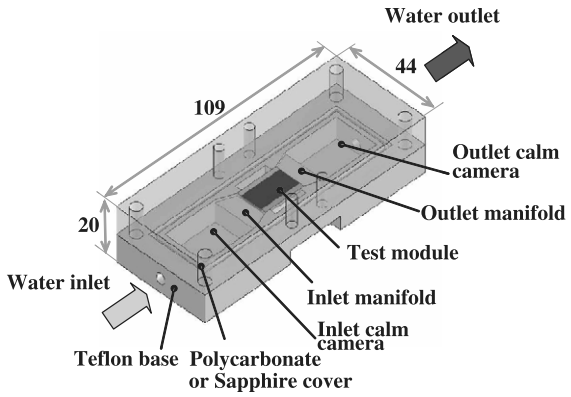

Fig. 2. Schematic view of the test section.

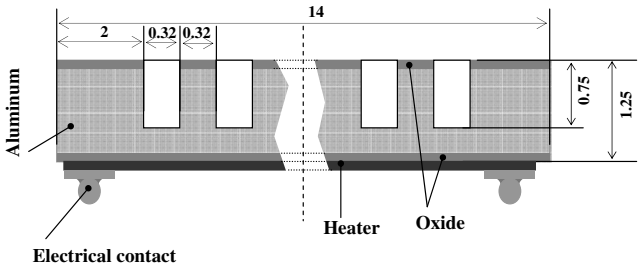

Fig. 3. Micro-channels cross-section.

test module is shown in Fig. 3. Sixteen micro-channels were machined on one side of this plate using a precision sawing technique. Electric resistor, which was used as a heat source, was located on the other side of the plate. The micro-channels were of 320 μm wide and 750 μm deep with an accuracy of ±10 μm. The serpentine pattern, electrical heater, $10 \times 10\ \text{mm}^2$ had been attached to the surface of the aluminum by chemical vapor deposition technique and provided a uniform heat flux. The heater filament, made of chrome, has dimensions of 1720 Å in thickness, 1.257 mm in width and length of 82 mm. The heat sink housing was made of Teflon in order to decrease the heat loses to the environment and keep the inlet/outlet manifolds temperature at constant value. A plate made of polycarbonate plastic was attached to the test section by several screws and served as transparent cover, which was used also for measurements of fluid temperature by thermocouples and for pressure drop measurements. During the measurements of fluid temperature into the micro-channels by IR technique a cover made of sapphire glass was employed. The transparent window of sapphire had a wave length range of 0.15–7 μm, which makes possible to perform visual observations and also IR measurements through the cover. When radiant energy strikes surface, a part of the radiation is reflected, part is absorbed and part is transmitted. The transmission of sapphire window at 10 mm thickness is shown in Fig. 4. From this figure one can conclude that the transmission is constant for most of the wavelength range. The transmission value for the wavelength of $\lambda = 5$ μm and $T = 273$ K is about 85%. This value of transmissivity makes possible measurements through sapphire by IR technique. Before these measurements a calibration procedure was conducted. In the range of given water temperature from 30 °C to 90 °C the water temperature moving into the manifolds was measured by thermocouples and by IR camera and then the calibration with an accuracy of ±1 K was performed.

2.2. Manifolds

Several studies [20,21] showed that the manifolds design play an important role in the liquid distribution among parallel micro-channels which can lead to spanwise temperature gradients on the device surface, enlarge thermal stresses and reduce his reliability. To study the effect of entrance conditions on temperature of the heater calculations using CFD software were conducted. Details of the calculation were described in [20,24]. Fig. 5 shows a typical temperature distribution on the heater. The fluid moves from the bottom to the top, the heat flux is $q = 4.4\ \text{W/cm}^2$ and the mass flux is $\dot{m} = 8.33\ \text{kg/m}^2\,\text{s}$. The figure presents a comparison between temperature field of the heater obtained from the numerical simulation (A) and that obtained from IR measurements (B). The square marked area of 10×10 mm shows the heater. Both of the pictures show very close temperature distribution. Fig. 6 shows the temperature distribution along the central and side lines, marked as lines 1, 2 respectively in Fig. 5. Numerical and experimental results agree quite well.

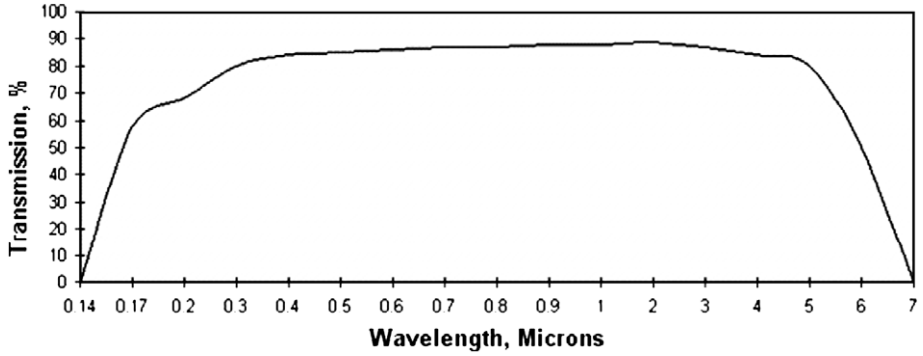

Fig. 4. Transmission vs. wave length at 10 mm thickness of Sapphire glass.

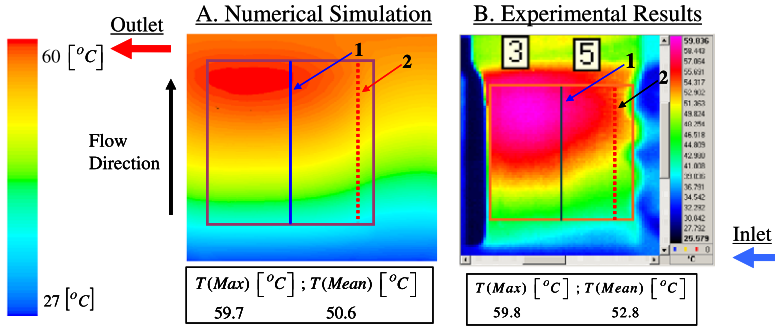

Fig. 5. Temperature field on the heater.

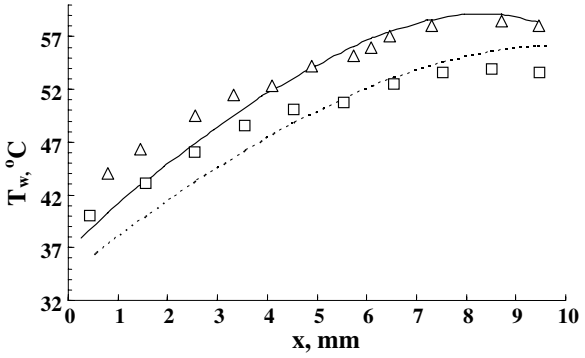

Fig. 6. Comparison between numerical simulation and experimental results for the temperature field on the heater surface: (—) simulation, (△) experimental results (line 1 in Fig. 5) (---) simulation, (□) experimental results (line 2 in Fig. 5).

To optimize the design of the manifold configuration, a number of numerical calculations were conducted. The calculations were carried out for three types of manifolds shown in Fig. 7. Fig. 8 shows the velocity distribution at the distance of 2 mm from the inlet to micro-channels for different types of the manifolds. From Fig. 8 one can conclude that configuration of the manifolds marked as 1 and 2 ensure uniform velocity distribution at the entrance to the micro-channels. In the present study the manifolds of type 1 were used.

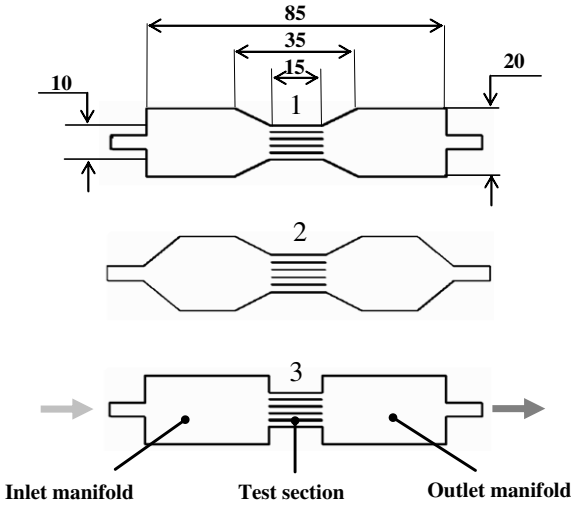

Fig. 7. Types of manifolds used for calculations.

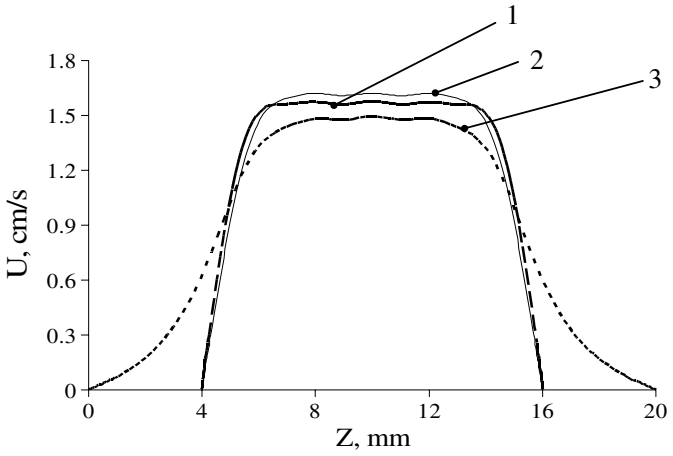

Fig. 8. Velocity profile at the micro-channel entrance. Manifolds: (1) type 1, (2) type 2, (3) type 3.

2.3. Measurement apparatus and procedure

A uniform heat flux, transferred by the electrical resistor, was controlled by a power supply. A thermal high-speed imaging radiometer was utilized to study the temperature field on the electrical heater and the working fluid temperature distribution along the micro-channels. The camera is suitable for temperature measurements in the wave length range of about 5 μm, The measurement resolution was of 0.03 mm. The heater was coated with a thin layer of black diffusive paint, with emissivity of 0.96. The determination of the emissivity was conducted through the method described in detail by Hetsroni et al. [22]. For pressure drop measurements the holes of diameter 0.6 mm were connected to pressure transducers by needles, Fig. 9. The pressure drop was measured directly at the central part of the micro-channels (not in the manifolds). Such a method makes possible to avoid pressure drop losses associated with contraction and expansion at the micro-channels inlet and outlet.

The data were collected by a digital data collecting system with an accuracy of ±1%. The temperature measuring process of the working fluid along the heated surface was divided in to two steps: at the first investigation, seven 0.3 mm T-type thermocouples were inserted into holes that were drilled in the plastic cover along the heat sink symme-

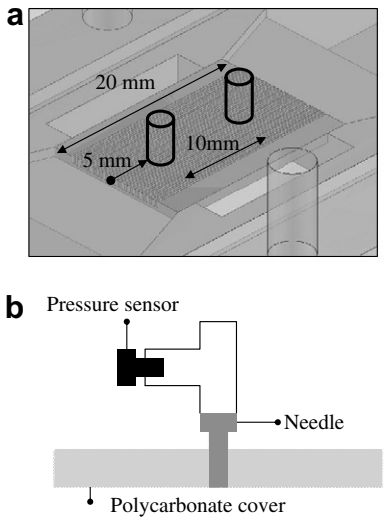

Fig. 9. Pressure measurements: (a) position of pressure sensors and (b) connection of pressure sensors.

try line, as shown in Fig. 10a. Fig. 10b shows the position of the thermocouple junctions relative to the micro-channel. The thermocouples measured the temperature of the thin fluid layer adjacent to the channel cover, as well as the IR readings,. The readings of the thermocouples were used to represent liquid balk temperature. These sensors measured the fluid bulk temperature in the manifolds as well as above the heater area. During the second step the fluid temperature was measured through the sapphire glass cover by IR camera with a microscopic lens. The matter is discussed in Section 2.5.

For normal testing procedure, the pump was turned on at mass flow rates from 0.3 g/s to 4.7 g/s. The electrical power to the heater was adjusted to a desired level by a variable voltage controller. The module was then allowed to reach a steady state, which was achieved within less than 5 min from the moment the flow conditions were stabilized. For each run values of mass flow rate and electric power were recorded by the data acquisition. Simultaneously the temperature of the water along the micro-channels was measured by thermocouples and the temperature field on the heater was recorded by the IR radiometer. These data were collected for 20 discrete values of Reynolds numbers in the range of $Re = 30$–600, and 5–8 different values of heat flux for a given Reynolds number. The plastic cover was then replaced by the sapphire glass and at the same experimental conditions the water temperature was measured by the IR radiometer. One of the advantages of this IR technique is continuous measurements of water temperature along the micro-channels and in the manifolds.

2.4. Data reduction

The bulk flow velocity was calculated as

$$u = m/\rho A \tag{1}$$

the friction factor was calculated as

$$f = 2\Delta p D_h / L \rho u^2 \tag{2}$$

The total heat input to the test module may be expressed as

$$N = N_1 + N_2 + N_3 \tag{3}$$

where N is the Joule heating in the heater, N_1 is the power transferred to the fluid in the channels, N_2 is the power conducted through the solid body of the test module in the axial direction, N_3 is the power dissipated due to heat losses.

The power generated by Joule heating was

$$N = IV \tag{4}$$

where I and V are the input current and voltage.

The power transferred to the fluid was estimated as

$$N_1 = mC_p(T_{out} - T_{in}) \tag{5}$$

where m is the mass flow rate, C_p is the specific heat, T_{out} and T_{in} are the outlet and the inlet temperatures measured by thermocouples T7 and T1, respectively.

For calculation of the average heat transfer coefficient the heat flux was assumed to be constant and was determined from the equation

$$q = N_1/F \tag{6}$$

where F is the heated surface of the micro-channels, which includes the bottom and the side walls. The average temperature on the heater, $T_{W(av)}$, and the average fluid temperature, $T_{f(av)}$ were used to calculate the average heat transfer coefficient and the average Nusselt number, $Nu_{(av)}$.

For determination of the local heat transfer coefficient the length of the heater was divided into number of sections and the local heat flux was calculated using Eq. (5), where T_{out} and T_{in} are the outlet and the inlet fluid temperatures at a given section measured by IR technique.

We assumed that at given cross-section the side-wall temperature of the micro-channel did not differ from the bottom temperature. The same assumption was used by Qu and Mudawar [26]. In this study the heat sink was fabricated from copper, consisted of an array of rectangular micro-channels of 231 μm wide, 713 μm deep and fitted with polycarbonate plastic cover plate. The measured temperature distributions showed good agreement with the corresponding numerical predictions. Lee et al. [33] measured the temperature on the bottom of micro-channels by thermocouples embedded in a copper test section. The temperature readings from these thermocouples were extrapolated to provide the average micro-channel wall temperature. For rectangular channels of $D_h = 318$–903 μm numerical predictions were found to be in good agreement with experimental data. Tiselj et al. [24] showed that due to the high thermal conductivity of the heat sink, the temperature field in the silicon wafer is close to isothermal one at each cross-section of triangular micro-channels with hydraulic diameter of 160 μm.

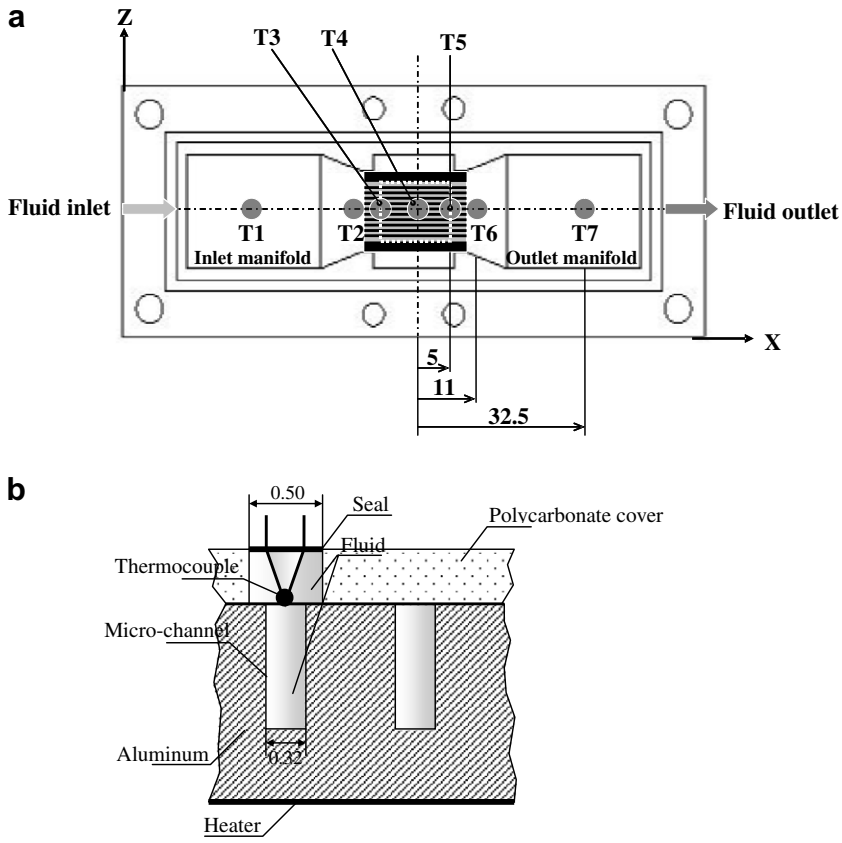

Fig. 10. Arrangement of thermocouples: (a) measurements by thermocouple and (b) thermocouple junction.

The local value of Nu is calculated by the following equation:

$$Nu = hD_h/k_f \tag{7}$$

The local heat transfer coefficient, h, was obtained using local heated channel wall temperature, T_W, and local fluid temperature, T_f, at the centers of a given section

$$h = q/(T_W - T_f) \tag{8}$$

The local fluid temperature, T_f, was determined by the IR technique. The following procedure was used to determine the wall temperature of the micro-channel from an infrared image of the heater. The straight lines on the bottom of the heated module corresponding to the streamwise axes of micro-channels were determined using the special image software. Along each line, the temperature on the heater was determined and then the temperature of the micro-channel bottom, T_W, was calculated from the heat conduction equation. It was assumed that the temperature distribution along the side walls did not differ significantly from that along the bottom. Temperatures used in the present study were averaged values obtained at the given cross-section for the channels placed at the central part of the test module. The bulk water temperature at given cross-section of the test module was used to calculate the physical fluid properties.

2.5. Verification of the method

For each steady-state experimental conditions an energy balance was performed. The average temperature of the heater and the average temperature of the Pyrex or sapphire cover were used to calculate the heat losses to ambient, N_3. The heat losses due to free convection and radiation were calculated. The electric power, N, and the power transferred to the fluid, N_1, were calculated using Eq. (4) and (5), respectively. The heat losses, N_3, due to free convection and radiation were calculated and then the power due to the axial heat flux, N_2, was determined from Eq. (3). It is important to stress that the heat losses were only a small fraction – between 0.5% and 1% of the total energy input from the heater.

The power N_2 may be also estimated from the measurements based on the temperature difference of (T6 − T2). In this case the power transferred to the fluid is

$$N_4 = mC_p(\mathrm{T6} - \mathrm{T2}) \tag{9}$$

where m is the mass flow rate.

Eq. (9) agrees with Eq. (5) with standard deviation of 4%. It should be noted that by the IR technique temperature of the thin fluid layer adjacent to the sapphire glass ($y = H$) was measured. We now consider a steady flow in micro-channel, with constant heat flux from below and constant wall temperature from the top. This problem

was studied numerically by Li and Cheng [34]. The results showed that if the height of micro-channel is larger then 10 μm the temperature gradient is quite small. Therefore, in a relatively high micro-channel, we can consider the temperature at $y = H$ in order to determine bulk fluid temperature.

The key question is: are the measurements of the fluid temperature carried out by the IR radiometer and by the thermocouples reflect the bulk temperature. We compared the power N transferred to the fluid from the measurements based on the temperature difference of (T5 – T3) to that based on the temperature difference of (T6 – T2). A good agreement was obtained.

3. Results and discussion

Experimental conditions are given in Tables 1–3.

3.1. Experimental uncertainty

The uncertainty of the components for an estimation of an error measurement of wall temperature was obtained according to the standard 1995 Guide to the Expression of Uncertainty of the Measurements [35]. The details of calculation are presented by Hetsroni et al. [22]. The error in determining the average Nusselt number, Nu, formed from an estimation of errors that became at measurements of the following values: D_h – the hydraulic diameter of the channels, L – the length of the channels, m – mass flow rate, $(T_{out} - T_{in})$ – difference between outlet and inlet temperatures of the liquid, $(T_{iw} - T_f)$ – difference between the averaged value of the inner wall and liquid temperatures as well as an error in the magnitude of the physical properties as C_p – specific heat of water and λ – thermal conductivity of water.

Table 1
Pressure drop measurements

N (–)	Mass flux (kg/m^2 s)	Inlet fluid temperature (°C)	Outlet fluid temperature (°C)	Pressure drop (Pa)
1	227	23.2	23.2	470
2	289	23.2	23.2	583
3	354	23.2	23.2	734
4	418	23.2	23.2	855
5	491	23.2	23.2	1040
6	560	23.3	23.3	1150
7	611	23.3	23.3	1290
8	677	23.3	23.3	1470
9	738	23.2	23.3	1600
10	815	23.2	23.2	1780
11	846	23.2	23.2	1870
12	921	23.3	23.3	2050
13	976	23.3	23.3	2240
14	1040	23.3	23.3	2430
15	1080	23.3	23.3	2580
16	1120	23.2	23.2	2710
17	1160	23.2	23.2	2760
18	1200	23.2	23.2	2920
19	1240	23.2	23.2	3050

Table 2
Average heat transfer measurements

N (–)	Mass flux (kg/m^2 s)	Inlet fluid temperature (°C)	Outlet fluid temperature (°C)	Average temperature on the bottom (°C)	Heat flux (W/m^2)
1	81.7	23.8	28.7	30.2	21,900
2	160	24.1	39.0	49.8	126,000
3	227	23.2	30.7	39.5	83,400
4	289	22.5	31.9	49.0	150,000
5	354	23.0	28.8	39.6	101,000
6	403	23.2	27.8	39.4	99,800
7	451	24.2	26.0	30.6	39,200
8	491	23.5	30.3	50.4	170,000
9	560	23.7	25.3	30.8	41,400
10	611	23.9	25.4	30.5	43,900
11	677	23.6	27.0	41.1	122,000
12	737	23.7	25.1	30.6	47,900
13	814	23.8	27.0	41.6	130,000
14	847	24.0	27.0	41.4	128,000
15	884	24.3	27.2	41.6	128,000
16	924	24.3	29.0	58.6	263,000
17	977	24.3	29.4	58.0	264,000
18	1080	24.2	29.0	56.6	264,000
19	1170	24.1	28.5	56.1	264,000
20	1240	23.9	28.0	54.6	264,000

Table 3
Local heat transfer measurements

N (–)	Mass flux (kg/m^2 s)	Distance from the inlet x (mm)	Temperature difference $\Delta T = T_W - T_f$ (°C)	Heat flux (W/m^2 K)
1	289	1	11.8	89,200
2		3	12.9	
3		5	13.7	
4		7	13.4	
5	451	0	10.0	105,000
6		1	12.1	
7		3	15.1	
8		5	15.2	
9		7	15.4	

The error of the product $f * Re$ is

$$\delta(fRe)/(fRe) = [(\delta\Delta P/\Delta P)^2 + (4\delta D_h/D_h)^2 + (\delta L/L)^2 + (\delta m/m)^2]^{0.5} \quad (10)$$

Eq. (10) shows that the channel hydraulic diameter measurement introduces some error into the uncertainty of the product $f * Re$.

The error in determining the power, N, generated by Joule heating is due to errors of measurements of both electric current and electric voltage. The error in magnitude of the power transferred to the working fluid, N_1, is due to uncertainties of the flow rate, m; specific heat of water, C_p, the difference between outlet and inlet temperatures $T_{out} - T_{in}$. The error in the estimation of heat losses, N_3, is due to correlations for calculation of natural convection and radiation heat transfer. Performing the error analysis according to [34] the uncertainties in determining various parameters in this study are given in Table 4.

Table 4
Experimental uncertainties (95% confidence level)

#	Source of uncertainty	Symbol	Uncertainty (%)
1	Hydraulic diameter	D_h	1.0
2	Length of the test section	L	0.3
3	Wall temperature	T_W	2.5
4	Difference between inlet and outlet temperatures of liquid	$T_{in} - T_{out}$	2.0
5	Difference between wall and liquid temperatures	$T_W - T_f$	3.0
6	Mass flow rate	$\dot{m}$	1.0
7	Electrical power	N	0.5
8	Power transferred to fluid	N_1	4.4
9	Power transferred trough tube wall	N_2	12.5
10	Heat losses	N_3	12.0
11	Heat transfer coefficient	h	13.0
12	Nusselt number	Nu	13.2
13	Friction coefficient	f	10.2
14	Reynolds number	Re	4.5
15	Specific heat of water	C_p	0.1
16	Thermal conductivity of water	k_f	0.5
17	Kinematic viscosity	v	2.1

3.2. Friction factor

3.2.1. The average Poiseuille number

Fig. 11 shows the dependence of Po on Re for the non-heated fluid flow. If the pressure drop is associated with the developing flow in smooth micro-channels the theoretical line for comparison would be a horizontal line. In the conventional theory, the relationships between the flow friction coefficient, f, and Reynolds number, Re, for fully developed laminar flow regime in rectangular channel may be calculated according to Shah and London [6]:

$$Po = 96(1 - 1.3553\alpha + 1.9467\alpha^2 - 1.7012\alpha^3 + 0.9564\alpha^4 - 0.2537\alpha^5) \quad (11)$$

where $\alpha = 0.4$ is the aspect ratio of the channel used in the present study.

The Poiseuille number calculated by Eq. (11) is $Po = 64.5$.

Many investigations have been concentrated on compact modeling methods for micro-channel heat sink. It is because numerical simulations and experiments require considerable effort and long time. An averaging approach was proposed by Kim and Kim [7]. The solution for the velocity distribution was obtained by solving one-dimensional averaged equations for fully developed flow. For $\alpha = 0.4$ the calculated Poiseuille number is about $Po = 56$.

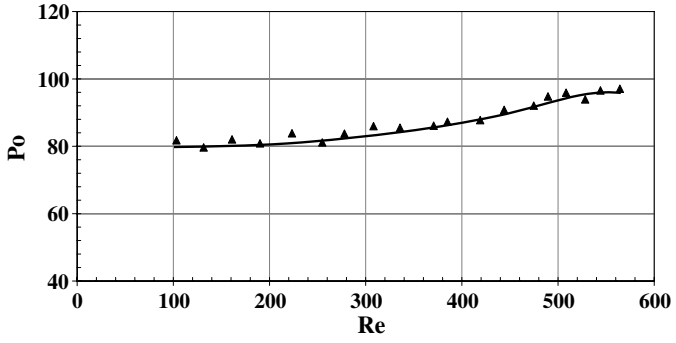

Fig. 11. Variation of the Poiseuille number with the Reynolds number.

The deviation of data from $Po = \text{const}$ could be misinterpreted as a transition to turbulence. The study of forced convection characteristics in rectangular channels with hydraulic diameter of 133–367 μm was performed by Peng and Peterson [9]. In these experiments the Reynolds number was in the range 50–4000. The main results of this study (and subsequent works, for example, Peng and Wang [10]) consisted of the following: (i) drag coefficients for laminar and turbulent flows are inversely proportional $Re^{1.98}$ and $Re^{1.72}$, respectively, (ii) Poiseuille number is not constant; for laminar flow it depends on Re, $Po \sim Re^{-0.98}$, (iii) the transition from laminar to turbulent flow occurs at Re about 300–700.

The hypothesis on earlier transition from laminar to turbulent flow in micro-tubes was presented by Mala and Li [14]. It is based on analysis of the nonlinear dependence of the pressure gradient on Reynolds number obtained in their experiments. Such a phenomenological analysis does not reveal the actual reasons of the displacement of boundary transition to low Reynolds numbers region. Kohl et al. [19] conducted an experimental investigation of microchannel flow with internal pressure measurements in the range of $4.9 < Re < 2068$. The measurements clearly showed the linear variation of pressure along the channel's length that is associated with laminar incompressible flow.

One of the possible ways to account for the influence of the roughness on the pressure drop in micro-tube is to apply a modified-viscosity model to calculate the velocity distribution. This model was proposed by Qu et al. [11] to interpret their experimental data. These results do not agree with those obtained in the present study and reported by other investigators [4,17,19]. Flows in micro-channels are often laminar, so the study of laminar flow in rough micro-channels has become important. High relative roughness may cause the Poiseuille number to vary with Re. It is known that hydraulically smooth flow regime occurs when the Reynolds number that is defined by height of roughness k_s and friction velocity u^* changes in the range $0 < k_s u^*/v < 5$ [4], the upper limit of this inequality determines the maximum value of the velocity at which laminar flow is possible. Taking into account that $u^* = (\tau/\rho)^{0.5}$, $\tau = \mu(du/dy)_w$, $u = u_m(1 - \eta^2)$, $\eta = r/r_0$ and $u_m = 2\bar{u}$ (τ is the shear stress at the wall, u_m and $\bar{u}$ are the maximum and average velocities, r_0 is the micro-channel radius, subscript w refers to wall), we arrive at the following estimate of the relative roughness, corresponding to the boundary that subdivides the flow in smooth and rough channels:

$$k_s/r_0 < 5/(1.4Re^{0.5}) \quad (12)$$

For $Re \sim 1000$, the relative roughness, that corresponds to the boundary between the smooth and roughness channels is $k_s/r_0 \sim 0.11$. The relative roughness of the bottom and

walls is calculated as k_s/r_0. The average roughness, ε, in this study was measured by optical profilometer and found as 4.3 μm, hence, the relative roughness is about 2%. The latter shows that hydraulic characteristics of micro-channels used in the present study are close to one of smooth micro-channels. The qualitative difference between the data by Peng and Wang [10], Qu et al. [11], Mala and Li [14] and theoretical predictions is, probably, due to experimental uncertainties.

3.2.2. Variation of the Poiseuille number vs. dimensionless length

The pressure drop between the inlet and the outlet of the channel was used to calculate Poiseuille number. For a given value of the channel size the Poiseuille number depends on the Reynolds number. This is obviously due to the finite thickness of the boundary layers at the channel entrance, as opposed to a uniform velocity profile in fully developed case. The inlet/outlet pressure measurements were also used by Gao et al. [30] and by Gamrat et al. [31] and it was shown that the dimensionless developing length X^+ is the proper parameter to take into account the entrance effects on the overall friction factor. Fig. 12 shows the variation of Poiseuille number vs. $X^+ = x/D_h Re$ for micro-channel roughness considered in the present study. The points show the results obtained in the range of Reynolds number $Re = 100$–580. The distribution of Po does not depend on Re. This result agrees with prediction for laminar developing flow channels of usual size, proposed by Shah and London [6]. Gamrat et al. [31] presented both two and three-dimensional numerical analysis of entrance effects on laminar liquid flow. The momentum and continuity equations were solved for the following hydraulic boundary conditions: a uniform velocity profile at the inlet container, the flow was assumed to be fully developed at the exit, no axial gradient for all the flow variables except pressure. It was found that distribution of $Po(x)$ depends on Re and channel spacing contrary to Shah and London [6] case where X^+ is the proper dimensionless group. The authors suggest that such effects are due to the finite thickness of the boundary layers at the channel entrance, as opposed to a uniform velocity profile in our experiments and the Shah and London [6] reference case.

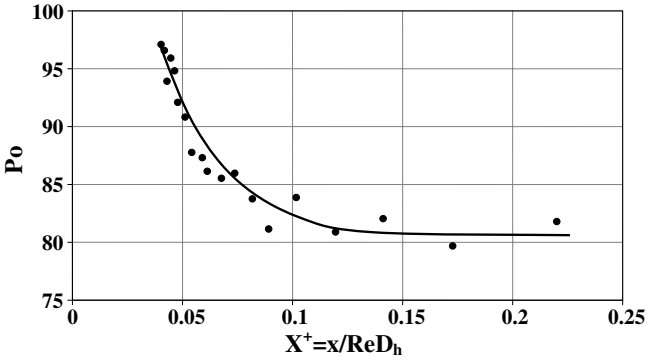

Fig. 12. Variation of the Poiseuille number against dimensionless length.

In the range of $X^+ < 0.01$ an increase in Re leads to an increase in Po [31]. The opposite effect was reported by Renksizbulut and Niazmand [25] where in the range of $X^+ < 0.01$ an increase in Re lead to a decrease in Po. The calculations were conducted for laminar flow in a trapezoidal channel. Inflow boundary conditions corresponded to a uniform flat velocity profile, for outflow zero gradients along the axial flow direction were applied to all variables. The results reported by Gamrat et al. [31] and by Renksizbulut and Niazmand [25] differ not only from the Shah and London [6] predictions but also from those obtained in the present study and in the study of Kohl et al. [19] where internal pressure measurements provide information about the pressure drop inside the channel.

While comparing the experimental results to those obtained by the conventional theory, it is most important to take into consideration the boundary condition of the problem. The comparison is correct only when those conditions are consistent. When dealing with fluid flow within micro-channels, in most applications, the short length of the channels is not enabling the flow to reach the fully developed regime. The dimensionless hydrodynamic length may be calculated as

$$L_h/D_h = 0.055Re \tag{13}$$

It is possible to formulate the general features of Poiseuille's flow as follows: $C^* = Po_{exp}/Po_{th}$, where Po_{exp} and Po_{th} are experimental and theoretical Poiseuille number, respectively. This condition testifies to identical form of the dependence of the experimental and theoretical drag coefficient on the Reynolds number.

Basically, there may be three reasons of the inconsistency between the theoretical and experimental friction factors: (i) discrepancy between the actual conditions of a given experiment and the assumptions used in deriving the theoretical value, (ii) error in measurements, (iii) effects due to decreasing the characteristic scale of the problem, which leads to changing correlation between the mass and surface forces.

The method presented by Shah and London [6] is used in the present study to determine the pressure drop associated with the developing flow in the entrance region of the channel. The effect of developing flow should be included in the theoretical model using Eq. (14):

$$(fRe)_{\text{Developing Flow}} = (fRe)_{\text{Fully Developed Flow}} + (K_\infty \rho u^2/2) \tag{14}$$

where K_∞ is the pressure loss coefficient associated with the developing flow. K_∞ was measured and calculated by previous researchers and the results were summarized by Shah and London [6]. In Fig. 13 – the experimental data of Po were normalized by values calculated for rectangular ducts according to Shah and London [6], Eq. (341). Fig. 13 shows the Poiseuille number calculated by Eq. (14). The experimental results agree with the analytical value within the data uncertainty.

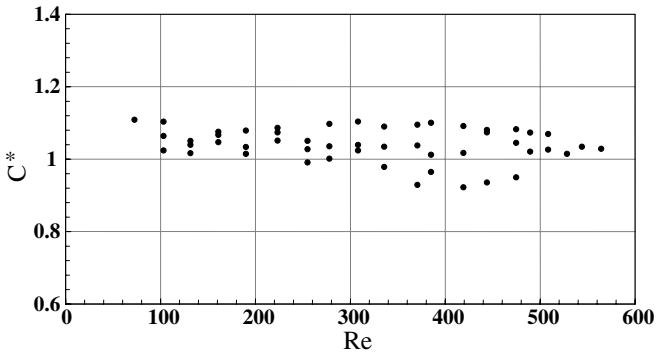

Fig. 13. Normalized Poiseuille number as a function of Reynolds number.

3.3. Thermal results

Comparison between heat balance based on difference between temperature of the fluid at the outlet and inlet manifolds and the temperature difference measured directly in the channel. It should be noted that when the heat balance is based on temperature difference (T6 − T2) the heated portion of the channels is shorter than the total length of the test section. Thermocouples T6 and T2 were placed into outlet and inlet calm chamber, respectively. When the measurements were conducted by thermocouples T5 and T3 the heated portion of the channels was the same as the channel length. These thermocouples were installed at the surface of the transparent cover adjoined to the top of the micro-channels. It was important to investigate the difference between temperature measured by thermocouples T5 and T3 and bulk temperature into the micro-channels. It should be also taken into account the heat transfer to the ambient, conducted through the thermo-electrodes and through the power wires connected to the power supply. This problem was especially serious in the case of comparison between the temperature measurements by thermocouples to those made by IR. The following value of ε was used as a measure STD of thermal uncertainty, ε, in the present experiment

$$\varepsilon = ((T6 - T2) - (T5 - T3))/(T6 - T2) \quad (15)$$

In the range $100 < Re < 580$ the value of STD was $\varepsilon = 8.4\%$. It depends on Reynolds number and decreases with an increase in Re. The results agree with heat balance data reported by Lelea et al. [27] for annular micro-channel of $D_h = 300$ μm. From both investigations it is clear that, as Re decreases, the outlet temperature of water increases. This results in an increase of the temperature of the thermo-electrodes and an increase of heat conduction through electrodes to the ambient.

3.3.1. Thermal visualization

The present study includes heat transfer aspects of the problem and relates both to the heater side problem and to thermal pattern into the micro-channels. The temperature distribution depends on the material and design of

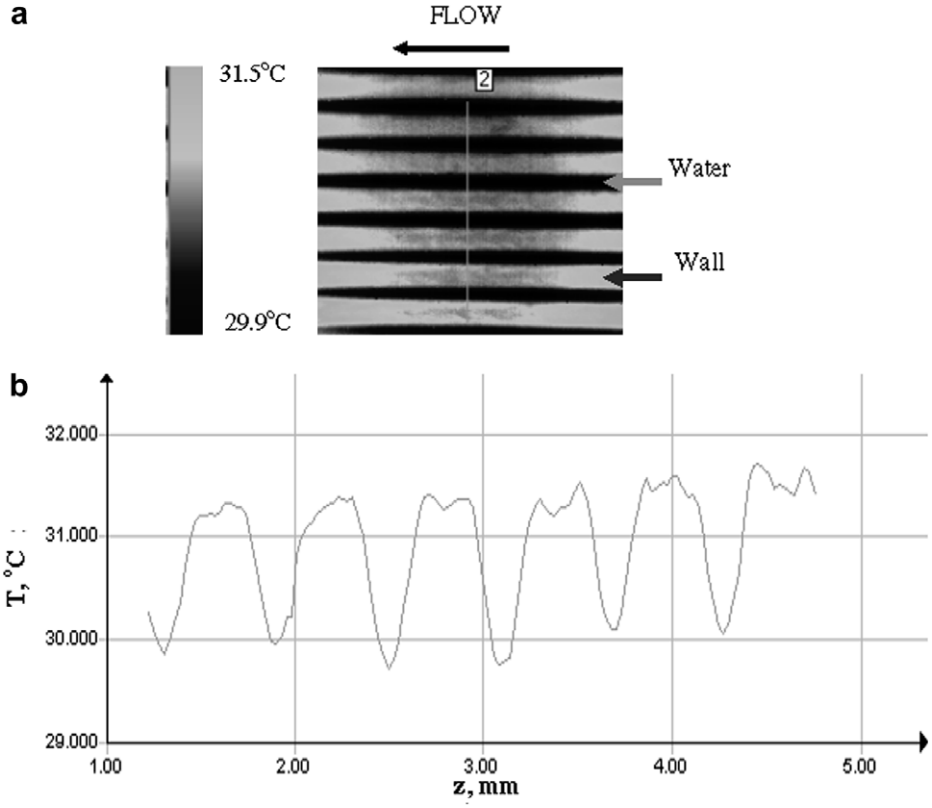

Fig. 14. Top view of the temperature field, $Re = 100$, $q = 25 \times 10^4$ W/m^2: (a) IR image and (b) temperature variation in the spanwise direction.

the module, flow rate into micro-channels and heat flux. For given values of flow rate and heat flux, the infra-red (IR) image at the surface of the transparent cover on top of the micro-channels was clearly observed. Fig. 14a shows the IR image (top view) of the central part of the test module obtained at mass flow rate $Re = 100$ and heat flux $q = 25.0 \times 10^4$ W/m^2. Fig. 14b shows the temperature distribution in the spanwise direction. The flow moved from the right to the left, the field of view is 3.6 mm and 3.6 mm in the streamwise and spanwise direction, respectively, the gray strips show the temperature on the channel walls (about 31.2 °C), the black strips show the temperature of the water (about 29.9 °C). The sequences of such images were used to determine the fluid temperature along the micro-channels.

3.3.2. Average Nusselt number

For heat transfer, the Prandtl number of the fluid also plays an important role. The thermal entrance may be calculated as

$$L_T/D_h = 0.055 Re Pr \quad (16)$$

The average Nusselt number as a function of the Reynolds number is presented in Fig. 15. Open circles represent Nu_{av} calculated using fluid temperatures measured by thermocouples T3, T4 and T5, closed circles represent Nu_{av} calculated using fluid temperatures measured by thermocouples T2 and T6, rectangular points represent Nu_{av} calculated using fluid temperatures measured by IR technique. The results of Shah and London [6] are also shown for comparison. In Fig. 15 – the solid line is based on data [6] – for the case of thermally developing and hydrodynamically developed flow, Table 51 [6]. As expected the experimental Nusselt number increases with the Reynolds number. Clearly, the length of the thermal entrance region increases with an increase in Re, the values in the entrance region are larger than those in the fully developed region, which highlights the critical importance of the entrance region in determining the heat transfer characteristics in micro-channel devices.

3.3.3. Local Nusselt number

In Fig. 16 the experimental results of the local value of Nu are plotted vs. the non-dimensional axial distance, $X^* = x/D_h Re Pr$ for the respective experimental conditions together with those reported by Warrier et al. [28]. Single-phase forced convection experiments have been performed by Warrier et al. [28]. The test section was made of aluminum and consisted of five parallel rectangular micro-channels of hydraulic diameter $D_h = 750$ μm and Re range of 557–1552. The measured values agree quite well with our data and numerical results, especially near the fully developed region. Close to the channel entrance the experimentally measured values generally tend to be about 25% lower. The experimental data in Fig. 16 indicate that the local Nu number decreases and approaches the constant value with increasing X^*. As seen from Fig. 16 the present experimental data are in reasonable agreement with theoretical results. It can be concluded that for rectangular micro-channels the local value of Nu is in good agreement with conventional theory including the entrance region. The same results were reported by Lelea et al. [27] on heat transfer and fluid flow of distilled water in micro-tubes of 0.1, 0.3, and 0.5 mm with Re number range up to 800.

Conduction and entrance effects on laminar liquid flow and heat transfer in rectangular micro-channels were investigated by Gamrat et al. [31]. Contrary to the results obtained in our study the variation of the measured Nu with the dimensionless coordinate are clearly depended on Re. For uniform inlet velocity and temperature profiles the effect of axial conduction in fluid on heat transfer essentially depends only at low Peclet numbers, Pe. It was shown by Petukhov [8] that at $Pe > 50$, $X^+ > 0.02$ the effect of axial conduction is less then 5%. At $Pe > 100$ this effect is negligibly small [8,25]. The experiments described by Gamrat et al. [31] were conducted in the range of $Re = 518$–2076 at Prandtl number about $Pr = 6$. The model used by the authors takes complex geometry and axial conduction effects in the solid wall into account. They assumed that

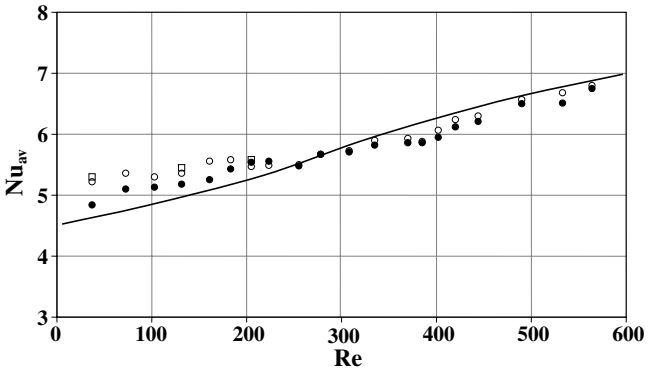

Fig. 15. Variation of the average Nusselt number with the Reynolds number: (○) data based on the fluid measurements by thermocouples T3, T4, T5, (●) data based on fluid measurements by thermocouples T2, T6, (□) data based on IR measurements, (—) Shah and London [6] solution.

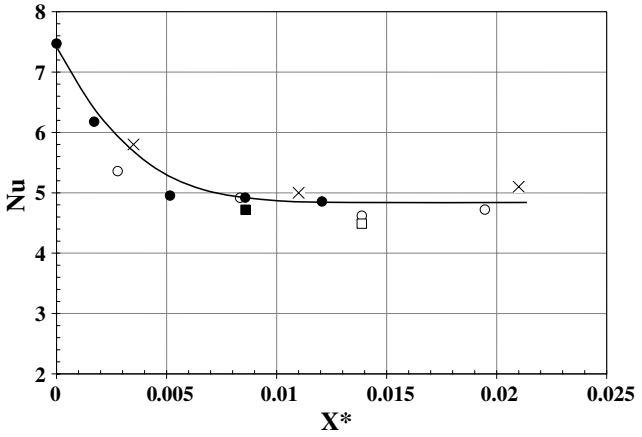

Fig. 16. Dependence of the local Nu on the dimensionless thermal entrance length. IR measurements: (○) $Re = 132$, (●) $Re = 205$, (□) measurements by thermocouples, (×) data by Warrier et al. [28].

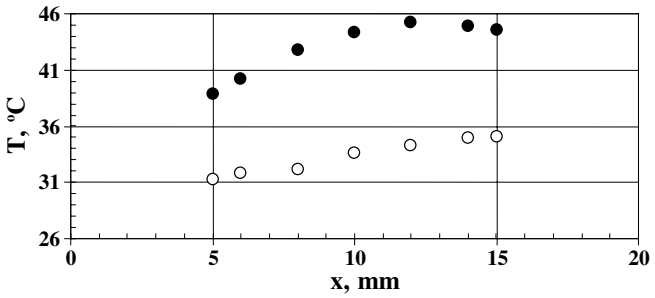

Fig. 17. Temperature distribution in the streamwise direction: (●) bottom temperature, (○) fluid temperature.

velocity and temperature profiles were *Re*-dependent at the micro-channel entrance.

3.3.4. Axial conduction in the wall

It is worth underlining that in the present study a convergent channel entrance was used, contrary to several other studies where the channel inlet is characterized by an abrupt contraction. As a consequence, nearly uniform velocity and temperature profiles at the inlet were achieved. IR technique made it possible to measure temperature distribution in the streamwise direction on the heater and in the fluid in the micro-channel. Fig. 17 shows the temperature distribution in the plane of symmetry at $Re = 30$ and $N = 19$ W. The wall temperature decreases in the last part of the micro-channel ($x/L > 0.75$) due to the lack of heating caused by axial conduction through the solid walls of the micro-channel. The wall and fluid bulk temperature distribution cannot be approximated as a linear one. Since measurements of the local heat flux were not possible in the present experimental study, we assumed that the heat flux into the test section was uniformly distributed in the spanwise direction. According to Tiselj et al. [24] the effect of non-uniform heat distribution leads to decrease in the local *Nu* in the part of micro-channel near the inlet.

4. Conclusion

The goal of this investigation has been to measure the pressure drop and temperature distribution of the flow in micro-channels in an attempt to determine the sources of unusual and often conflicting results previously reported in the literature. The new method that was used provides information about the fluid temperature distribution inside the channel and provides validation for the methods used to determine the local and average Nusselt numbers.

A developing micro-channel heat transfer and fluid flow has been investigated experimentally on rectangular micro-channels of $D_h = 440$ μm, having water as a working fluid. The experimental results have been compared with theoretical predictions from literature and results obtained by numerical modeling of the present experiment. The experimental results of pressure drop and heat transfer confirm that including the entrance effects, the conventional theory is applicable for water flow through micro-channels.

It was shown that data presented by other researches can be carried over to entrance effects. The present results highlight the importance of accounting for common phenomena that are often negligible for standard flows such as accounting for profile of inlet velocity, axial heat conduction, effect of the design inlet and outlet manifolds.

References

[1] D.B. Tuckerman, R.F. Pease, High performance heat sinking for VLSI, IEEE Electron Dev. Lett., EDL-2 (5) (1998) 126–129.
[2] C.B. Sobhan, S.V. Garimella, A comparative analysis of studies on heat transfer and fluid flow in micro-channels, Microscale Thermophys. Eng. 5 (2001) 293–311.
[3] G.L. Morini, Single-phase convective heat transfer in microchannels: a review of experimental results, Int. J. Therm. Sci. 43 (2004) 631–651.
[4] G. Hetsroni, A. Mosyak, E. Pogrebnyak, L.P. Yarin, Fluid flow in micro-channels, Int. J. Heat Mass Transfer 48 (10) (2005) 1982–1998.
[5] G. Hetsroni, A. Mosyak, E. Pogrebnyak, L.P. Yarin, Heat transfer in micro-channel, Int. J. Heat Mass Transfer 48 (25–26) (2005) 5580–5601.
[6] R.K. Shah, A.L. London, Laminar Flow Forced Convection in Ducts, Academic Press, New York, 1978, S.V.
[7] D.K. Kim, S.J. Kim, Averaging approach for micro-channel heat sinks subject to the uniform wall temperature condition, Int. J. Heat Mass Transfer 49 (2006) 695–706.
[8] B.S. Petukhov, Heat transfer and drag of laminar flow of liquid pipes. Energy, Moscow, 1967.
[9] X.F. Peng, G.P. Peterson, Convective heat transfer and friction for water flow in micro-channel structures, Int. J. Heat Mass Transfer 39 (1996) 2599–2608.
[10] X.F. Peng, B.X. Wang, Forced convection and boiling characteristics in micro-channels, in: Heat Transfer 1998 Proceedings of 11th IHTC, vol. 11, Kyongiu, Korea, August 1998, pp. 371–390.
[11] W. Qu, M. Mala, Pressure-driven water flow in trapezoidal silicon micro-channels, Int. J. Heat Mass Transfer 43 (2000) 353–364.
[12] D. Pfund, D. Rector, A. Shekarriz, A. Popescu, J. Welty, Pressure drop measurements in microchannel, AIChe J. 46 (8) (2000) 1496–1507.
[13] P.X. Jiang, M.H. Fan, G.S. Si, Z.P. Ren, Thermal-hydraulic performance of small scale micro-channel and porous-media heat-exchangers, Int. J. Heat Mass Transfer 44 (2001) 1039–1051.
[14] Gh.M. Mala, D. Li, Flow characteristics of water in micro-tubes, Int. J. Heat Fluid Flow 20 (1999) 142–148.
[15] S.G. Kandlikar, S. Joshi, S. Tian, Effect of surface roughness on heat transfer and fluid flow characteristics at low Reynolds number in small diameter tubes, Heat Transfer Eng. 24 (3) (2003) 4–16.
[16] B. Xu, K.T. Ooi, N.T. Wong, W.K. Choi, Experimental investigation of flow friction for liquid flow in microchannels, Int. Commun. Heat Mass Transfer 27 (8) (2000) 1165–1176.
[17] K.V. Sharp, R.J. Adrian, Transition from laminar to turbulent flow in liquid filled micro-tubes, Exp. Fluids 36 (2004) 741–747.
[18] Z-Y. Guo, Z-X. Li, Size effect on micro-scale single-phase flow and heat transfer, Int. J. Heat Mass Transfer 46 (2003) 149–159.
[19] M.J. Kohl, S.I. Abdel-Khalik, S.M. Jeter, D.L. Sadowski, An experimental investigation of microchannel flow with internal pressure measurements, Int. J. Heat Mass Transfer 48 (2005) 1518–1533.
[20] D. Klein, G. Hetsroni, A. Mosyak, Heat transfer characteristics of water and APG surfactant solution in a micro-channel heat sink, Int. J. Multiphase Flow 31 (2005) 393–415.
[21] Z. Zhang, Y. Li, CFD simulation on inlet configuration of plate-fin heat exchangers, Cryogenics 43 (12) (2003) 673–678.

[22] G. Hetsroni, M. Gurevich, A. Mosyak, R. Rozenblit, Surface temperature measurements of a heated capillary tube by means of an infrared technique, Measur. Sci. Technol. 14 (2003) 807–814.
[23] M.M. Rahman, Measurements of heat transfer in microchannel heat sinks, Int. Commun. Heat Mass Transfer 27 (4) (2000) 495–506.
[24] I. Tiselj, G. Hetsroni, B. Mavko, A. Mosyak, E. Pogrebnyak, Z. Segal, Effect of axial conduction on the heat transfer in microchannels, Int. J. Heat Mass Transfer 47 (2004) 2551–2565.
[25] M. Renksizbulut, H. Niazmand, Laminar flow and heat transfer in the entrance region of trapezoidal channels with constant wall temperature, J. Heat Transfer 128 (2006) 63–74.
[26] W. Qu, I. Mudawar, Experimental and numerical study of pressure drop and heat transfer in a single-phase micro-channel heat sink, Int. J. Heat Mass Transfer 45 (2002) 2549–2565.
[27] D. Lelea, S. Nishio, K. Takano, The experimental research on microtube heat transfer and fluid flow of distilled water, Int. J. Heat Mass Transfer 47 (2004) 2817–2830.
[28] G.R. Warrier, V.K. Dhir, L.A. Momoda, Heat transfer and pressure drop in narrow rectangular channels, Exp. Therm. Fluid Sci. 26 (2002) 53–64.
[29] W.M. Kays, M.E. Krawford, Convective Heat and Mass Transfer, McGraw-Hill, New York, 1993.
[30] P. Gao, S.L. Person, M. Favre-Marient, Scale effects on hydrodynamics and heat transfer in two-dimensional mini and microchannels, Int. J. Therm. Sci. 41 (2002) 1017–1027.
[31] G. Gamrat, M. Favre-Marient, D. Asendrych, Conduction and entrance effects on laminar liquid flow and heat transfer in rectangular microchannels, Int. J. Heat Mass Transfer 48 (2005) 2943–2954.
[32] J.L. Xu, Y.H. Gan, D.C. Zhang, X.H. Li, Microscale heat transfer enhancement using thermal boundary layer redeveloping concept, Int. J. Heat Mass Transfer 48 (2005) 1662–1674.
[33] P.S. Lee, S.V. Garimella, D. Liu, Investigation of heat transfer in rectangular microchannels, Int. J. Heat Mass Transfer 48 (2005) 1688–1704.
[34] J. Li, P. Cheng, Bubble cavitation in micro-channel, Int. J. Heat Mass Transfer 47 (2004) 2689–2698.
[35] Guide to the Expression of Uncertainty of Measurement, Geneva, International Organization for Standardization, 1995.